

# Fast transit portal dosimetry using density-scaled layer modeling of aSi-based electronic portal imaging device and Monte Carlo method

Jae Won Jung

*Department of Physics, East Carolina University, Greenville, North Carolina 27858*

Jong Oh Kim

*Department of Radiation Oncology, University of Pittsburgh Cancer Institute, Pittsburgh, Pennsylvania 15232*

Inhwan Jason Yeo<sup>a)</sup>

*Department of Radiation Medicine, Loma Linda University Medical Center, Loma Linda, California 92354*

Young-Bin Cho and Sun Mo Kim

*Department of Radiation Oncology, Princess Margaret Hospital, Toronto, Ontario M5G 2M9, Canada*

Steven DiBiase

*Department of Radiation Oncology, Robert Wood Johnson School of Medicine, Camden, New Jersey 08103*

(Received 14 December 2011; revised 2 October 2012; accepted for publication 15 October 2012; published 29 November 2012)

**Purpose:** Fast and accurate transit portal dosimetry was investigated by developing a density-scaled layer model of electronic portal imaging device (EPID) and applying it to a clinical environment.

**Methods:** The model was developed for fast Monte Carlo dose calculation. The model was validated through comparison with measurements of dose on EPID using first open beams of varying field sizes under a 20-cm-thick flat phantom. After this basic validation, the model was further tested by applying it to transit dosimetry and dose reconstruction that employed our predetermined dose-response-based algorithm developed earlier. The application employed clinical intensity-modulated beams irradiated on a Rando phantom. The clinical beams were obtained through planning on pelvic regions of the Rando phantom simulating prostate and large pelvis intensity modulated radiation therapy. To enhance agreement between calculations and measurements of dose near penumbral regions, convolution conversion of acquired EPID images was alternatively used. In addition, thickness-dependent image-to-dose calibration factors were generated through measurements of image and calculations of dose in EPID through flat phantoms of various thicknesses. The factors were used to convert acquired images in EPID into dose.

**Results:** For open beam measurements, the model showed agreement with measurements in dose difference better than 2% across open fields. For tests with a Rando phantom, the transit dosimetry measurements were compared with forwardly calculated doses in EPID showing gamma pass rates between 90.8% and 98.8% given 4.5 mm distance-to-agreement (DTA) and 3% dose difference (DD) for all individual beams tried in this study. The reconstructed dose in the phantom was compared with forwardly calculated doses showing pass rates between 93.3% and 100% in isocentric perpendicular planes to the beam direction given 3 mm DTA and 3% DD for all beams. On isocentric axial planes, the pass rates varied between 95.8% and 99.9% for all individual beams and they were 98.2% and 99.9% for the composite beams of the small and large pelvis cases, respectively. Three-dimensional gamma pass rates were 99.0% and 96.4% for the small and large pelvis cases, respectively.

**Conclusions:** The layer model of EPID built for Monte Carlo calculations offered fast (less than 1 min) and accurate calculation for transit dosimetry and dose reconstruction. © 2012 American Association of Physicists in Medicine. [<http://dx.doi.org/10.1118/1.4764563>]

Key words: electronic portal imaging device, dose reconstruction, portal dosimetry, Monte Carlo methods

## I. INTRODUCTION

As a mechanism of external radiation delivery has been advanced by implementation of sophisticated techniques, such as intensity modulated radiation therapy (IMRT) or volumetric intensity modulated arc therapy (VMAT), verification of delivered dose into a patient has been gaining more importance. As a result, continuous efforts have been made in the

developments of dose verification techniques using online measurement devices.<sup>1-6</sup> In these efforts, the use of an on-board imager, electronic portal imaging device (EPID), has been receiving wide interests as it offers dosimetric measurement with superior spatial resolution as well as portal imaging performance.<sup>5-13</sup>

Comparisons between measurements and treatment planning calculations on EPID are widely used in verification of

dose delivery using EPID without patient involvement.<sup>5,6,14–16</sup> The absence of patient makes the verification simple in terms of measurement and calculation, but such verification does not allow evaluating dose distributions in patient.

In order to take real patient into account, therefore, dose verification using transit imaging has been widely performed.<sup>6,7,10–12,17–19</sup> In this regards, several dose verification techniques using transit images have been proposed that include transit image evaluation<sup>13,15,16</sup> and dose reconstruction in patient volume.<sup>14,17–19</sup>

For dosimetry using transit imaging and dose reconstruction alike, computation models and associated algorithms play critical roles in prediction of portal dose image accurately. Efforts have been, therefore, made to develop them for EPIDs based on liquid-ion-chamber (LIC) matrix and amorphous silicon (aSi)-based flat panel. When LIC-based EPIDs were introduced, investigators successfully developed computational models (i.e., homogeneous models) and algorithms for it achieving comparable results to film or ion-chamber measurement.<sup>7–11,13,14</sup> This was possible because the LIC-based EPID responds water-equivalently.

While the LIC-based EPID has been diminishing from clinical use, aSi-based EPIDs have become more popular portal imagers due to their superior imaging capabilities. Although the addition of high-atomic-number components of aSi-based EPIDs enhances imaging performance, it works counter-productively in reproducing water-equivalent dose. Furthermore, bringing patient into portal imaging calculation introduces difficulty in predicting the transit EPID image due to scattered radiation that increases as the patient thickness increases. Overcoming such disparity and difficulty have been at the center of investigators' efforts on developing accurate and fast EPID models and calculation algorithms. Addressing this issue, McCurdy *et al.*<sup>20,21</sup> have predetermined dose deposition kernels on a build-up metal and phosphor (gadolinium oxysulfide) layers of aSi-based EPID. They modeled portal dose images then by convolving the kernels to photon fluences that were separately predicted between primary and scattered photons in the plane of EPID. The prediction of the scattered photons was based on predetermined scatter kernels by Monte Carlo calculations on flat phantoms of various thicknesses. On the other hand, in order to extract the primary photon fluence from EPID measurements, Patridge *et al.*<sup>19</sup> have employed measured parameters and precalculated scatter kernels (Monte Carlo) in a relation<sup>22</sup> of portal dose images to primary and scatter components. Employing an additional iterative model<sup>23,24</sup> that relates the primary to the scatter component, the primary fluence was then determined and subsequently used to calculate dose in a patient.

Predetermination of the scatter contribution to portal dose images was continued by van Elmpt *et al.*<sup>25</sup> They have used a lateral scatter kernel that was calculated from phantom-scatter measurements to extract primary energy fluence from portal dose images obtained without a patient object. The primary fluence after ray-tracing was later used to calculate in-phantom doses. van Elmpt *et al.*<sup>12</sup> additionally performed dose reconstruction employing the predetermined kernel and the lat-

eral scatter kernel discussed above. Steciw *et al.*<sup>26</sup> have also predetermined dose deposition kernel in the phosphor layer of the EPID. They extracted primary fluences by deconvolving EPID dose images obtained without a patient object with the kernel, and used them for dose calculation in the patient. Jarry and Verhaegen<sup>27</sup> have modeled the EPID in detail using the BEAMnrc Monte Carlo code system and predetermined dose deposition in the phosphor layer. By using scattered EPID dose images from patient's planning images, they extracted primary photon fluences from treatment EPID images, through which dose was reconstructed.

The approaches by the above investigators on transit dosimetry or dose reconstruction involving patient are indirect dose prediction methods based on fluence and dose-deposition-kernel-based modeling and are characterized by how the scatter component of photons that reaches EPIDs is modeled. They used either measurements or calculations to predetermine the scatter component in terms of kernels or other parameters in the dose model of EPIDs. In this regard, instead of employing such indirect dose prediction models, the direct prediction of the EPID dose image, through full radiation transport calculations of the energy deposition by all contributing particles including primary and scattered photons and electrons, may be a reasonable alternative and a more accurate approach to consider.

This study intends to directly predict the EPID dose image under patient and reconstruct dose in patient utilizing full particle transport for portal image as well as patient dose calculations. The full particle transport is designed to offer accurate and relatively fast primary and scattered photon transport calculations through patient and air gap, down to EPID. Details of the EPID dose image prediction and dose reconstruction are described in our prior work.<sup>18</sup> The calculation down to EPID with a patient, however, requires much higher computing resources (time and accuracy) than the calculation without patient. In order to achieve fast calculation of portal dose using a Monte Carlo code, XVMC (Ref. 28) was employed in calculation of patient dose and EPID image. In order to overcome the lack of modeling of high-atomic number elements in XVMC, a density-scaled homogeneous layer model of EPID is introduced and an appropriate commissioning method using a meta dose quantity is proposed. For this purpose, this study aims at appropriately modeling the EPID for image prediction and applying it to clinical use such as transit portal dosimetry and dose reconstruction.

## II. MATERIALS AND METHODS

### II.A. EPID modeling with XVMC

#### II.A.1. Homogeneous layer model

Because XVMC was originally developed for Monte Carlo dose calculation in voxelized tissue-like media, it does not offer physics model of high-atomic number materials, such as phosphor and copper plates, that constitute an amorphous silicon imager.<sup>28</sup> It also limits physical modeling of imager's thin parts into fixed-size voxelized geometry. Therefore, in order to build a model of imager using XVMC, the imaging part

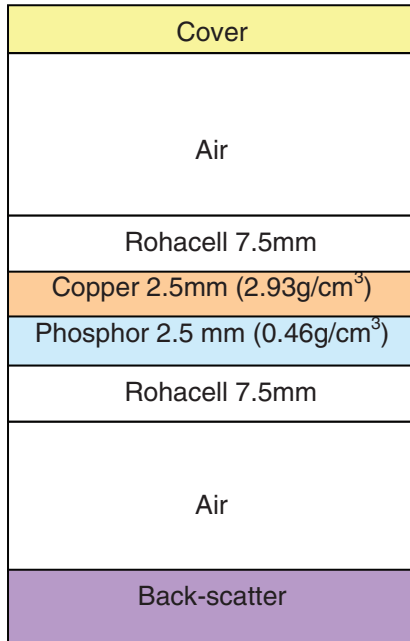


FIG. 1. EPID model in XVMC. A simplified diagram of the homogeneous EPID model is provided in this figure and the actual modeling employed details (material content, thickness, and density) from the manufacturer. The Phosphor was based on Gadolinium Oxy Sulfide.

of Varian's aS1000 (Varian Medical Systems, Inc., Palo Alto, CA) was scaled into multiple homogeneous layers with effective densities as shown in Fig. 1. We chose 2.5 mm as the voxel dimension in the direction of beam through the patient to the portal imager. Homogenizing process of each layer adjusted the thickness of imager elements to the nearest multiples of the voxel dimension and scaled the density of imager elements to the effective density which restores the same area density of elements (details are available by Varian Medical Systems, Inc., Palo Alto, CA).

Very thin layers of the original elements were not included in the model except those associated with high density. Thin layers with high densities were fitted to the smallest available layer thickness, i.e., 2.5 mm by the density scaling. A uniform slab layer below the EPID was used without detailed modeling of the supporting arm as supported by Siebers *et al.*<sup>5</sup> Because the response of the light sensor is proportional to energy deposition in the phosphor, the EPID dose image was computed by acquiring the energy deposition scored in the phosphor. The EPID model using XVMC was validated through comparison with measurements for various sizes of open fields with a flat phantom.

### II.A.2. EPID calibration

In order to relate images acquired in EPID to the dose calculated in the above model, the images needed to be calibrated and converted into dose. First of all, variant pixel outputs of EPID were corrected following a step utilized by Siebers *et al.*<sup>5</sup> Portal images were acquired in an integrated dose acquisition mode of Varian IAS3 software on a Varian aS1000 under a 6 MV photon beam from a Varian Clinac 23iX (Varian

Medical Systems, Palo Alto, CA). A flood field (an open beam of  $22.0 \times 16.4 \text{ cm}^2$ ) was flattened by passing through a 20 cm thick water-equivalent solid phantom on couch at a distance of 90 cm SSD. The EPID was positioned at a large source-to-detector distance (SDD) of 185 cm, so that the flat beam profile could uniformly cover the imager. The use of such flat flood field enables measurement of actual beam horns on beam profiles.

After the flood field calibration, an image-to-dose calibration was performed. This calibration will convert acquired images to meta (dose) images to be compared with XVMC calculated images. An open field covering the whole imaging area was measured in EPID and calculated in the EPID model that was positioned at 150 cm SDD under a 20 cm solid water flat phantom (RMI phantom, Gammex<sup>®</sup>, Middleton, WI,  $40 \times 40 \text{ cm}^2$  area) at 90 cm SSD. For calculation, the flat phantom was CT-scanned and imported into the XVMC code. The dose calculations were performed throughout this study at the resolution of  $0.25 \times 0.3 \times 0.25 \text{ cm}^3$  which could offer statistically reliable results in a reasonable amount of calculation time. The calculated dose profiles were resampled by using bicubic interpolation in the MATLAB software (The MathWorks Inc., Natick, MA) to match the resolution and dimensions of the MC calculated EPID signal to the measured signal. The measured images were then aligned with the calculated profiles using an inhouse image alignment tool based on least-square optimization. The ratio of calculated image to measured image constituted a two-dimensional matrix of image correction factors as shown in Eq. (1). To cover the maximum area, a largest open beam ( $22.0 \times 16.4 \text{ cm}^2$ ) that covers the imaging plate of EPID was employed for this study

$$CM_n(i, j) = \frac{OF_{\text{calc}}(i, j)}{OF_m(i, j)}, \quad (1)$$

where,  $i$  and  $j$  are spatial indices in the cross- and inplane-directions of aS1000, respectively;  $OF_{\text{calc}}(i, j)$  is the calculated pixel dose at  $i$  and  $j$  on XVMC dose plane for the open field; and  $OF_m(i, j)$  is the measured pixel value at  $i$  and  $j$  on EPID image for the same field. Note that  $OF_{\text{calc}}(i, j)$  and  $OF_m(i, j)$  are normalized quantities, and thus  $CM_n(i, j)$  do not assume any absolute output ratio value. An absolute value was given to  $CM_n(i, j)$  by the ratio of  $OF_{\text{calc}}^{\text{ref}}$  to  $OF_m^{\text{ref}}$  averaged over the central  $1 \times 1 \text{ cm}^2$  area of EPID image for the reference field (open  $20 \times 20 \text{ cm}^2$  field) under a 20 cm flat phantom as shown in Eq. (2),

$$CM(i, j) = CM_n(i, j) \times \frac{OF_{\text{calc}}^{\text{ref}}}{OF_m^{\text{ref}}}, \quad (2)$$

where  $CM(i, j)$  is the calibration matrix that converts pixel values of EPID images into meta (dose) values. In theory, adjustment of output is not necessary if the calculation model is perfect. The simplified model of EPID geometry and materials used in this study provides a small field-size dependence of output variation ( $<2\%$ ), justifying the use of one representative field for output ratio determination.

Application of  $CM(i, j)$  to measured images  $I_m$  as shown in Eq. (3) converts them to dose in EPID,

$$E_{\text{corrected}}(i, j) = I_m(i, j) \times CM(i, j), \quad (3)$$

where  $E_{\text{corrected}}(i, j)$  is the corrected pixel dose at  $i$  and  $j$ ;  $I_m(i, j)$  is the measured pixel value at  $i$  and  $j$  on the EPID image. This process contributes to minimizing the discrepancies between measured and calculated images in EPID that could originate from the limitations of the calculation model from the treatment accelerator head to the EPID. Note that this favorably compromises the asymmetric image responses of aS1000 along inplane direction due to the presence of the supporting arm for dose evaluation because such asymmetry was calibrated to a symmetric, calculated dose profile on the layer model with which measured EPID images are compared. Note also that this asymmetry is not a serious problem because backscattered photons are much less significant than forwardly scattered photons from phantom.<sup>29</sup>

Although the layer model of EPID offers fast calculation, the fact that layers of high-atomic number elements were modeled to thicker dimensions limited by the utilized voxel size and high-atomic numbers were not modeled may have caused smoother penumbra profiles than measurements. To improve the penumbral agreement,  $E_{\text{corrected}}(i, j)$  were convoluted using a Gaussian kernel as shown in Eq. (4),

$$E_{\text{convoluted}}(i, j) = E_{\text{corrected}}(i, j) \otimes K(i, j), \quad (4)$$

where  $K(i, j)$  is a convolution kernel;  $E_{\text{convoluted}}(i, j)$  is a convoluted meta (dose) image. The convolution kernel was pre-determined by conv2 command of MATLAB for a standard field of  $10 \times 10 \text{ cm}^2$  until the best agreement is achieved in penumbra by iteratively adjusting the standard deviation term of the Gaussian kernel (determined to be 1.2), and then verified across various field sizes ( $5 \times 5 - 20 \times 20 \text{ cm}^2$ ). Note that quantity of the convoluted meta image is dose to imaging layer in the XVMC model. The calculated dose image and the meta dose image were compared as shown in Fig. 2.

## II.B. Validation of EPID model

### II.B.1. Open fields on flat phantom

The EPID model was validated through measurement employing open fields and flat phantoms as a first step of valida-

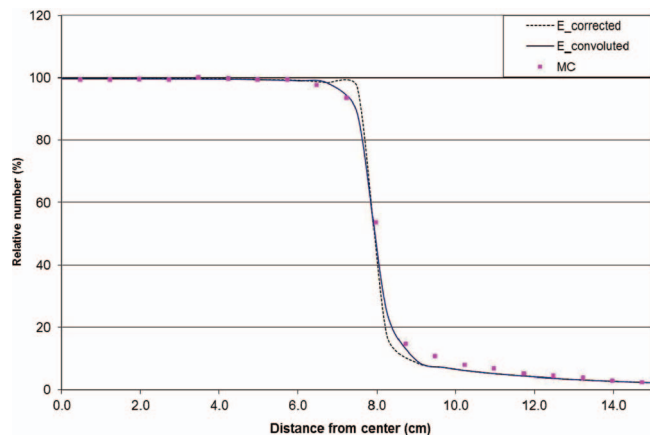


FIG. 2. Comparison of profiles in EPID that were corrected from measurements ( $E_{\text{corrected}}$ ), processed thru convolution ( $E_{\text{convoluted}}$ ), and Monte Carlo (MC)-calculated for  $10 \times 10 \text{ cm}^2$ .

tion. Images were calculated and measured for several open fields ( $5 \times 5, 7 \times 7, 10 \times 10, 15 \times 15, 20 \times 20 \text{ cm}^2$ ) on the EPID that was placed at 150 cm with a 20 cm-thick phantom (simulating patient) at 90 cm SSD. The EPID images  $I_m$  in DICOM format were transferred to a local computer for processing based on the above equations which were programmed in inhouse MATLAB scripts. Comparison between computation and measurement of EPID images was done by profile overlaying in inplane and crossplane directions. The maximum difference of EPID images was calculated within the central 80% of the field width. In order to determine the variability of image agreement to calculated dose with the phantom thickness changes, the phantom thicknesses were additionally varied from 10 to 38 cm.

## II.C. Application

### II.C.1. IMRT fields on Rando phantom

The clinical application of the EPID model in the transit dosimetry was done using a Rando phantom and clinical IMRT fields. A computed tomography (CT) image of Rando phantom was acquired and converted into a voxelized patient volume using a CT number-to-density table. The volume was then combined with the EPID model for XVMC simulation. Inhouse software was used in these processes.

Two IMRT plans were created for prostate and pelvis cancer in Rando phantom for demonstration of the transit dosimetry using EPID images. Five fields IMRT was optimized for prostate cancer treatment with the maximum field size of  $10 \times 6 \text{ cm}^2$  representing a small field size. Four fields IMRT was optimized for pelvis cancer treatment with the maximum field of  $14 \times 16 \text{ cm}^2$  representing a medium-to-large field size. The Rando patient was set on couch at 92.0 cm SSD and the EPID was placed at 150.0 cm as a normal megavoltage imaging position. Figure 3 is a screen capture displaying crosssections of the patient and the EPID in XVMC modeling. XVMC simulated photons and electrons entering into and exiting from the patient volume. The exiting

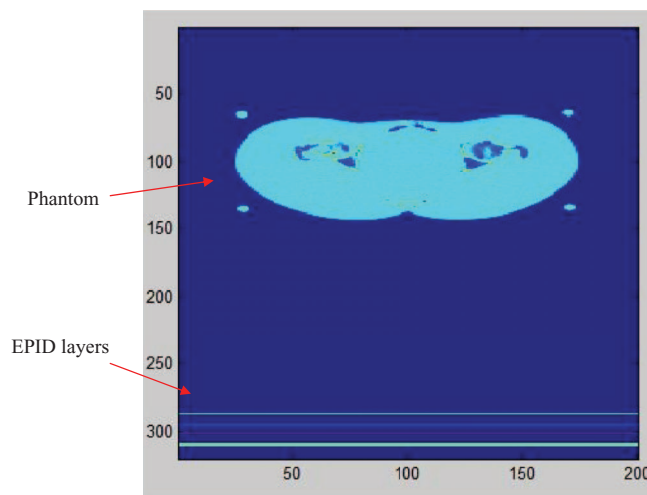


FIG. 3. Computation setup of phantom and EPID in the XVMC code. Under the Rando phantom are EPID layers that are shown in detail in Fig. 1.

particles travel air until they reach and interact in the EPID. Comparison between computation and measurement of two-dimensional EPID image as well as profile comparison and gamma analysis<sup>30</sup> was performed. The dose images were imported into MapCHECK software (Sun Nuclear, Inc.) for evaluation.

### II.C.2. Dose reconstruction: Advanced clinical use

For each field, following the methods and steps entailed in the dose reconstruction process in our prior work,<sup>18</sup> dose reconstruction was performed. Equation (5) and following explanations briefly describe how to reconstruct patient dose  $P$  using a meta dose image of EPID from measurement  $E_{\text{convoluted}}$  and precalculated dose responses in patient  $R_p$  and in EPID  $R_e$ ,

$$\underline{P} = \underline{R}_p / \underline{R}_e \cdot \underline{E}_{\text{convoluted}}, \quad (5)$$

where the underline of each term imply matrix. The linearity is provided by full-scope Monte Carlo response calculation of a treatment condition defined by beam delivery parameters (MLC positions), a patient, and EPID. Dose reconstruction steps based on the method included (A) forward calculation of two-dimensional dose responses in EPID,  $R_e$ , and three-dimensional responses in the phantom,  $R_p$ , for each beam used in treatment delivery; (B) measurement of transit radiation in EPID  $I_m$  and image processing through Eq. (4); (C) forward calculation of dose image in EPID and comparison with measured dose image  $E_{\text{convoluted}}$  for validation of radiation delivery (note: transit dose images can be constructed by convolving the precalculated  $R_e$  by the intensities of a given field); (D) inverse reconstruction of dose in patient,  $P$  using Eq. (5). The entire beam opening was modeled as one beam (i.e., global beam calculation discussed later). For the above calculations, a Varian 120 leaf MLC model in XVMC was used, that contains tongue-and-groove and rounded leaf tip modeling. The reconstructed and forward-calculated 3D dose profiles were compared by using dose volume histogram and 2D and 3D gamma analyses.

## III. RESULTS AND DISCUSSIONS

### III.A. EPID modeling with XVMC

The layer model of EPID was developed, calibrated, and processed by convolution as discussed in the method section. Figure 2 compares profiles in EPID that were directly measured ( $E_{\text{corrected}}$ ), processed through convolution ( $E_{\text{convoluted}}$ ), and MC-calculated for  $10 \times 10 \text{ cm}^2$  field size. The MC calculation overestimated dose outside penumbra after convolution, while the overestimation was less than 4% of the maximum dose. The figure showed good agreement within 1% between the calculation and the measurement in open-beam and penumbral areas. When the computing speed (i.e., CPU upgrades and multiple processing) reaches to an acceptable level for clinical use, we may be able to model elemental composition of EPID directly under patient.

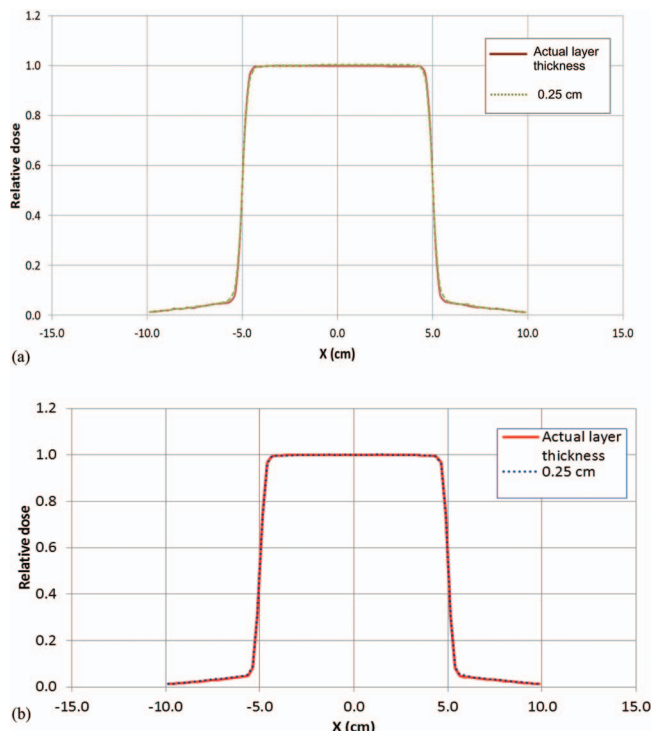


FIG. 4. Beam profile comparison of phosphor (a) and copper (b) layers with different thicknesses. The actual phosphor and copper thicknesses in EPID and 0.25 cm were compared. A beam of 6 MV and  $10 \times 10 \text{ cm}^2$  was used.

Figure 4 shows profile comparison between the layers of the actual phosphor and copper thicknesses (a propriety information, Varian Medical Systems, Inc.) and the density-scaled layers to fit one voxel dimension (0.25 cm). The dose sampling distance was 100 cm to the layer of phosphor under the irradiation of 6 MV beam with  $10 \times 10 \text{ cm}^2$  field size. As the thicknesses increased to 0.25 cm, it is natural to expect x-ray path length increase and electron spread. However, the figure shows otherwise, implying that the spatial spread in our EPID model is due to the lack of elemental composition modeling. The convolution in Eq. (4) corrects for such limitation of the model.

### III.B. Validation of EPID model

#### III.B.1. Open fields on flat phantom

The dose responses at phantom and EPID throughout this study were calculated on dual six core 2.93 GHz Intel XEON CPUs and 12.0 GB RAM. The calculation time was less than 1 min per beam. Figures 5 and 6 compare measured ( $E_{\text{corrected}}$  and  $E_{\text{convoluted}}$ ) and calculated profiles at 150 cm in the directions of cross- and inplanes, respectively, of open fields of various sizes under a 20-cm phantom at 90 cm SSD. Note that these are absolute dose comparisons between the two. The observed agreement was better than 2% within infield regions. The maximum difference was observed for  $5 \times 5 \text{ cm}^2$ . The small deviation observed in Figs. 5 and 6 can be attributed to the statistical

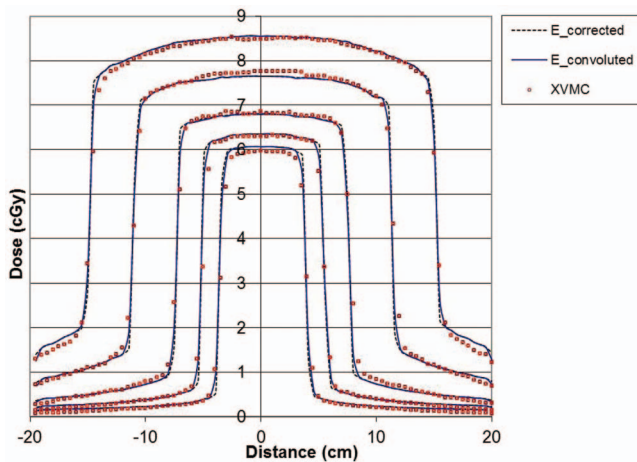


FIG. 5. Beam profile comparison in the crossplane direction between calculations (XVMC) and measurements ( $E_{corrected}$  and  $E_{convoluted}$ ) at 150 cm under a 20-cm flat phantom for various field sizes. The measured profiles have been processed through convolution. The phantom was placed at 90 cm SSD. The profiles are for field sizes of  $5 \times 5$ ,  $7 \times 7$ ,  $10 \times 10$ ,  $15 \times 15$ , and  $20 \times 20$  cm<sup>2</sup>.

uncertainty of the MC simulation and the imperfect agreement near the penumbrae.

Even when phantom thicknesses were varied, for each phantom thickness the agreement was achieved within 2.0% difference across infield regions for various field sizes. The layer model of EPID without modeling elemental composition and backscatter such as the arm structure could provide an acceptable agreement. The thickness variation between 20 and 38 cm caused 4%–5% image-to-dose response variation of the EPID model developed in this study as shown in Fig. 7. The thickness-dependent calibration factors in Fig. 7 that corresponds to the average external thickness of the phantom and the field size for each IMRT beams were, therefore, used. Such thickness determination has a minimal impact on the

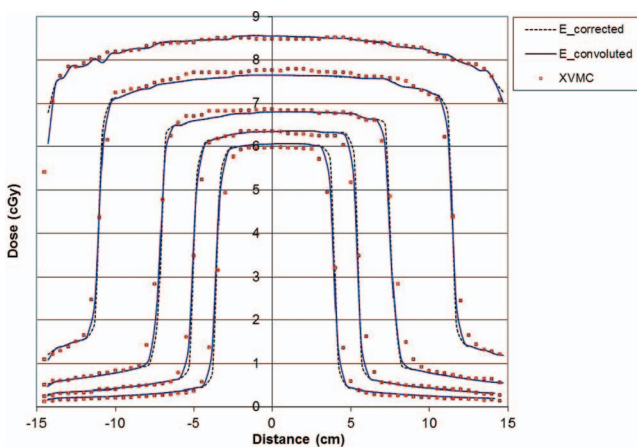


FIG. 6. Beam profile comparison in the inplane direction between calculations (XVMC) and measurements ( $E_{corrected}$  and  $E_{convoluted}$ ) in EPID at 150 cm for various field sizes under a 20-cm flat phantom. The measured profiles have been processed through convolution. The phantom was placed at 90 cm SSD. The profiles are for field sizes of  $5 \times 5$ ,  $7 \times 7$ ,  $10 \times 10$ ,  $15 \times 15$ , and  $20 \times 20$  cm<sup>2</sup>.

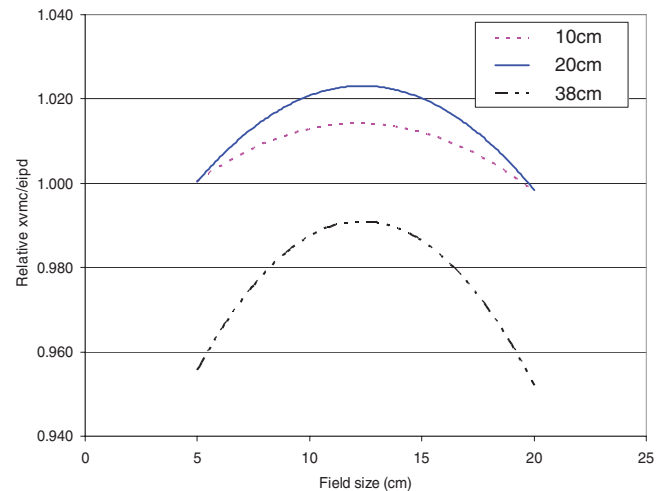


FIG. 7. Image-to-dose conversion factor of EPID dependent on phantom thicknesses. The data are normalized to the datum for  $20 \times 20$  cm<sup>2</sup> (set to one).

calibration as the thicknesses of the phantom near the irradiated site vary a little.

### III.C. Application

#### III.C.1. IMRT fields on Rando phantom

Figure 8 demonstrate the accuracy of the EPID model which was developed in this study and validated in Figs. 5 and 6. Figure 8 compares the calculated dose distribution with the measured,  $E_{corrected}$  and  $E_{convoluted}$  in EPID for an IMRT beam of a 6 MV photon that was incident on the Rando phantom from the anterior-to-posterior direction. The calculated dose agreed well with the measured dose in the infield region. In the comparison, 91.8% and 97.3% of dose points passed the gamma test given the criteria of 3% DD and 4.5 mm (equivalent to 3 mm at 100 cm) distance-to-agreement (DTA), respectively. For the gamma test, we have used dose evaluation software in MapCHECK (Sun Nuclear, Inc., Melbourne, FL).

#### III.C.2. Dose reconstruction

Figure 9 compares the reconstructed dose distribution with the forward-calculated dose distribution in the perpendicular isocentric plane to the beam direction within the Rando phantom for the same beam. They agreed well in the infield region. In the comparison, 96.7% of dose points passed the gamma test given the criteria of 3% DD or 3 mm DTA. We have only included the dose points greater than 10% of the dose maximum for the evaluation.

Table I shows Gamma pass rates for all beams tested in this study in EPID and within the Rando phantom in both perpendicular and axial planes. They varied between 90.8% and 98.8% given the criteria of 3% DD and 4.5 mm DTA in EPID and between 93.3% and 100% dose points given 3% DD or 3 mm DTA in the phantom. The variance was between 91.8% and 98.1% when the kernel was not convolved [Eq. (4)] in EPID. Figure 10 shows the composite reconstructed dose

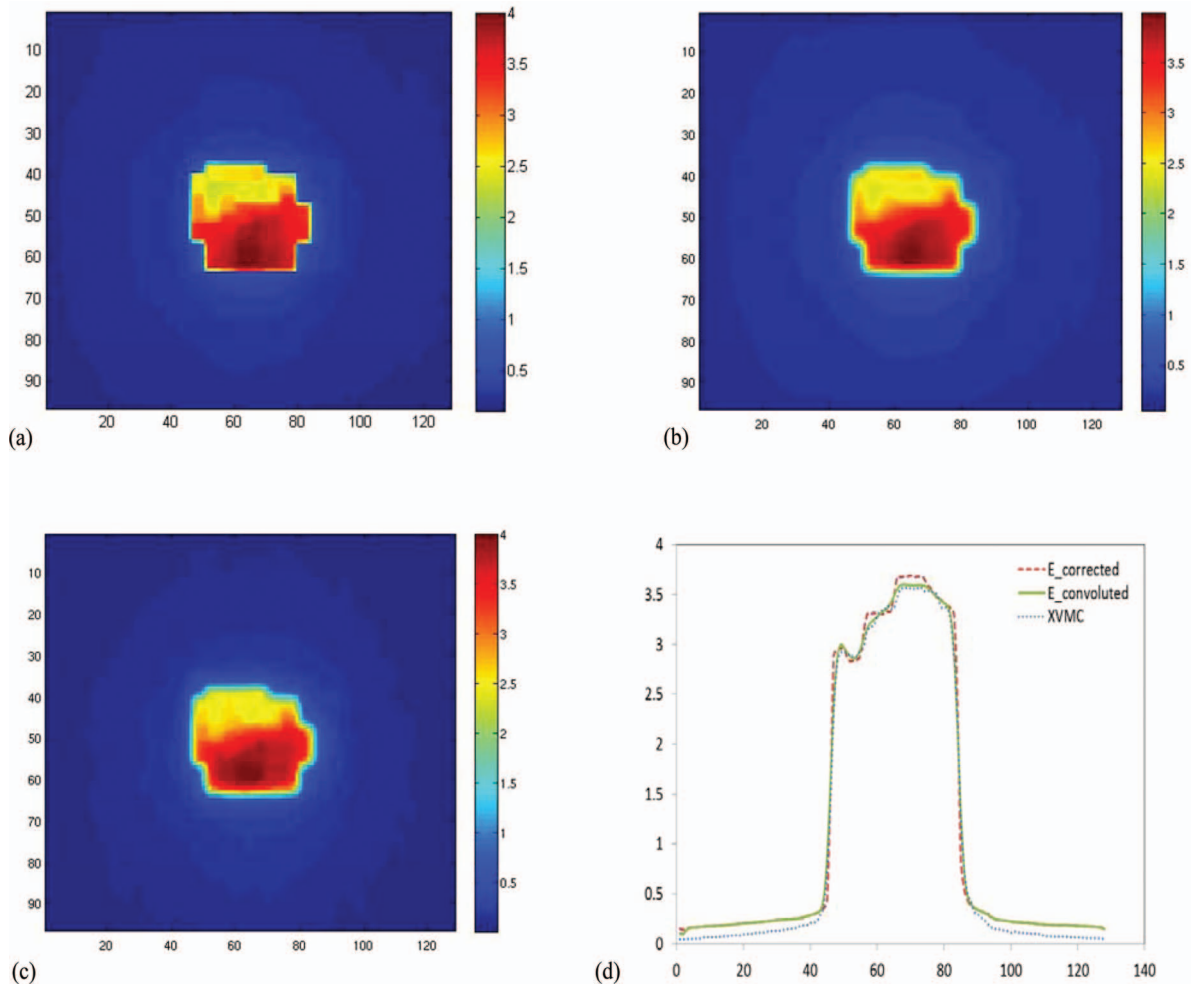


FIG. 8. Dose distribution comparison in EPID for an IMRT beam incident from  $0^\circ$  angle. Horizontal and vertical indexes are pixel numbers. (a) Measured dose distribution ( $E_{corrected}$ ), (b) measured dose distribution after convolution ( $E_{convolved}$ ), (c) calculated dose distribution, (d) dose profile comparison at  $y = 49$ . The dose points above 10% isodose line were selected for quantitative dose evaluation.

TABLE I. Pass-rates(%) of forwardly calculated and reconstructed doses for IMRT beams. In EPID, both measured dose images ( $E_{corrected}$  and  $E_{convolved}$ ) were employed for comparison. The dose points above 10% isodose line were selected for quantitative dose evaluation. The criteria of 3% DD and 4.5 mm DTA were used for evaluation of forward-calculated dose in EPID at 150 cm. The criteria of 3% DD and 3.0 mm DTA were used for evaluation of reconstructed dose in an isocentric plane at 100 cm within the phantom.

		$E_{corrected}/E_{convolved}$ in EPID (150 cm)	in Phantom (isocenter)	
			Perpendicular plane	Axial plane
Prostate	AP( $0^\circ$ )	91.8%/97.3%	96.7%	97.4%
	LAO( $33^\circ$ )	94.4%/93.1%	93.3%	97.6%
	LPO( $97^\circ$ )	94.6%/98.8%	100.0%	99.6%
	RAO( $327^\circ$ )	93.7%/98.4%	99.6%	98.4%
	RPO( $263^\circ$ )	94.6%/96.1%	100.0%	95.8%
	Composite			98.2%
Whole pelvis	AP( $0^\circ$ )	95.5%/97.0%	96.2%	99.9%
	LL( $90^\circ$ )	85.5%/90.8%	99.1%	99.9%
	PA( $180^\circ$ )	92.0%/94.7%	95.9%	99.1%
	RL( $270^\circ$ )	92.3%/95.1%	94.0%	99.9%
	Composite			99.9%

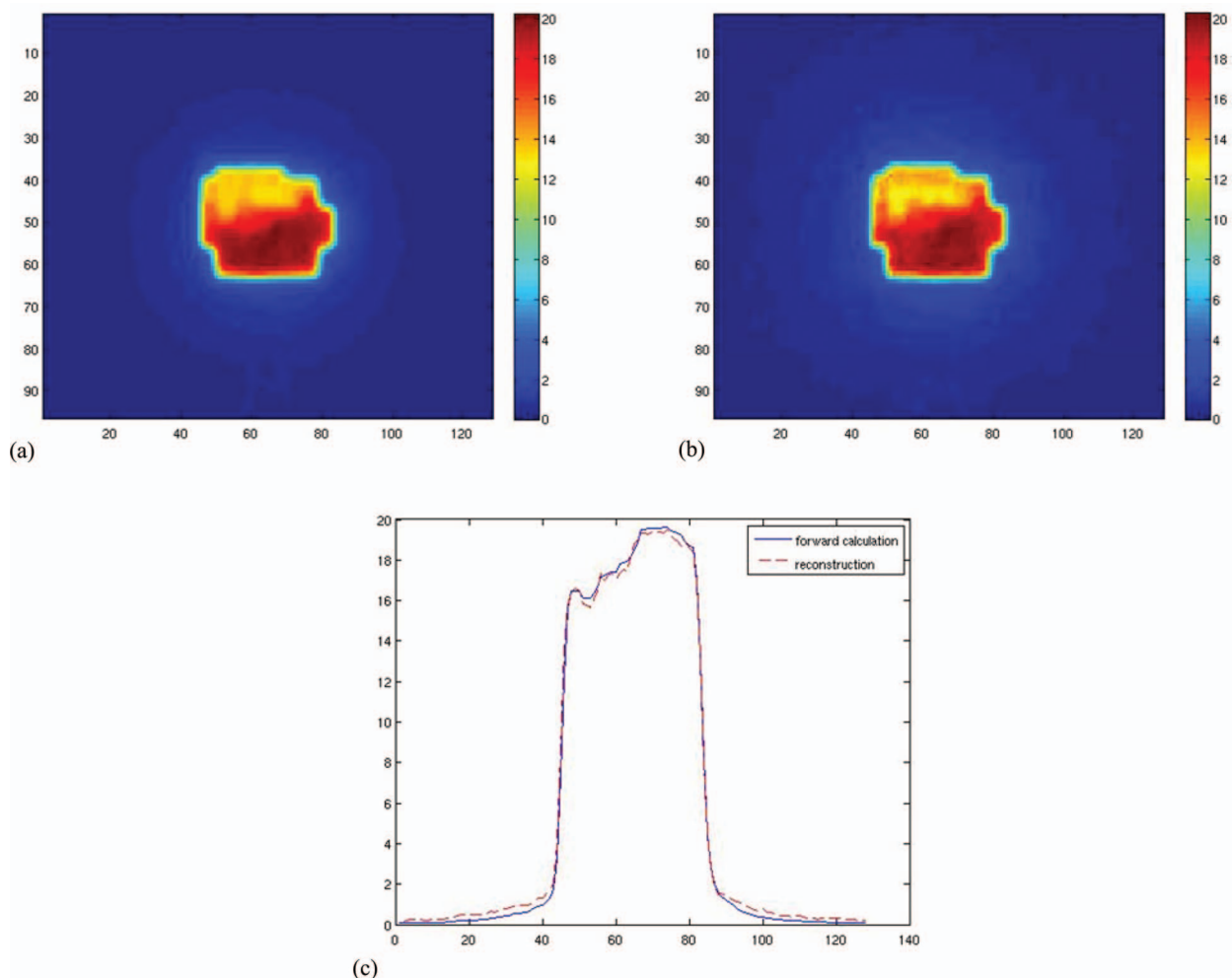


FIG. 9. Dose distribution comparison on an isocentric plane in the Rando phantom for an IMRT beam incident from  $0^\circ$  angle. (a) Calculated dose distribution, (b) reconstructed dose distribution, (c) dose profile comparison at  $y = 49$ . The dose points above 10% isodose line were selected for quantitative dose evaluation.

distribution compared with the forwardly calculated dose distribution for the small and large prostate cases. Figure 11 shows anatomical evaluation of the reconstructed dose distribution in terms of dose volume histogram comparing it with the forward distribution for each organ of interests. The pass rates of 3D gamma (3%, 3 mm, 10% threshold) were 99.0% and 96.4% for small field and large field, respectively. The reconstructed dose distribution agreed well with the forward calculated dose profiles. The layer model developed in this study combined with the convolution resulted in fast and reasonably accurate calculation of dose deposition in EPID and dose reconstruction in phantom as well. Our method of dose reconstruction can construct forwardly calculated doses in EPID, through the use of dose responses that were predetermined for dose reconstruction.<sup>18</sup> So, it can perform both transit dosimetry and dose reconstruction as well. Note that the accuracy (or agreement) of dose reconstruction generally reflects that of the forward transit dosimetry, which is due to the linear nature of the reconstruction algorithm.<sup>18</sup> However, when transit dosimetry generated disagreement in penumbra to the extent depicted in Fig. 2, the reconstruction algorithm based on direct inversion from dose image in EPID to inphan-

tom dose tends to enhance error (disagreement) in penumbral areas. This leads to low pass rates for relatively small radiation fields in which penumbral areas take a major part of the entire irradiated areas. Therefore, the reconstruction without the kernel use was not pursued. This poor performance did not come from the EPID model we developed, but the dose reconstruction algorithm we have employed.

As a part of the global beam calculation processes for dose reconstruction in this study, the calculation voxels in EPID were later resized, such that they are aligned to the voxels in phantom along beam emission/divergence lines. This was necessary to computationally match the matrix dimension of each term in the equation for dose reconstruction and to establish a relationship between the responses in phantom and EPID. Such implementation of the global beam calculation offered faster calculation. Note that the virtual beamlet calculations on which our previous work is based<sup>18</sup> and the global beam calculations produce in principle identical results of dose reconstruction to each other only limited by calculational noise characteristics.

The motivation of this research was to achieve maximum accuracy by employing full particle transport and at the same

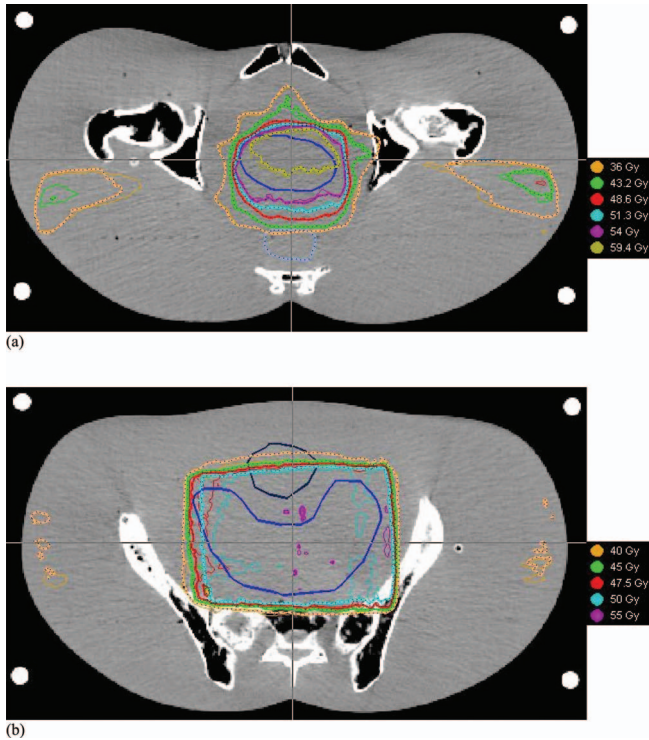


FIG. 10. Comparison of the forwardly calculated dose distribution (thick) with the inversely reconstructed dose distribution (thin) for (a) small field plan and (b) large field plan.

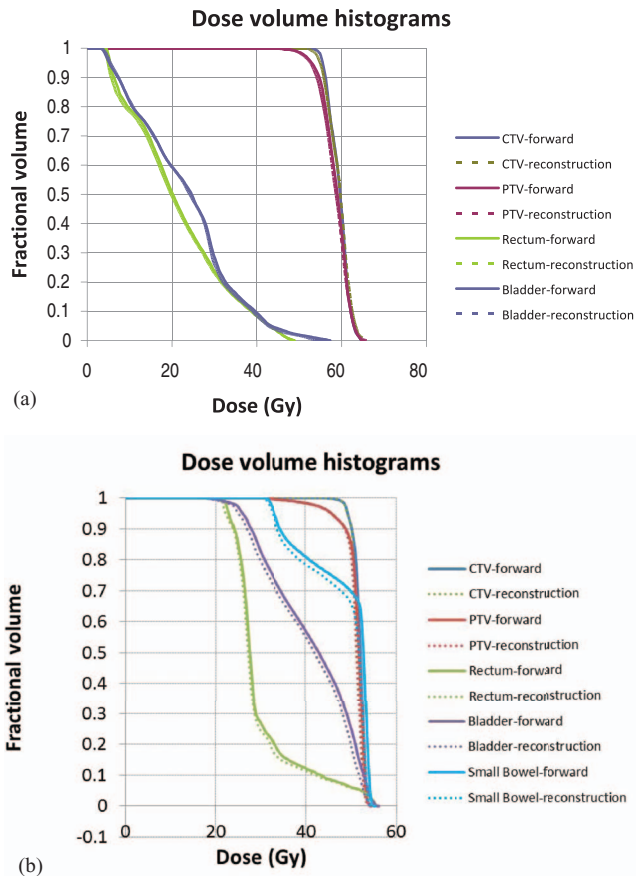


FIG. 11. Dose volume histograms for (a) small prostate case and (b) large pelvis case.

time to achieve a relatively fast calculation in transit dosimetry and dose reconstruction. Therefore, we have developed a density-scaled layer model of aSi EPID without modeling elemental composition within the framework of Monte Carlo calculations based on XVMC code. Within this motivation, the layer modeling has greatly exploited the speed of calculation, while the utilization of the Gaussian kernel improved the overall agreement in EPID. Note that the use of the precalculated kernel (to account for the influence of scattering) has been adopted by other studies (discussed in the Introduction) in which convolution dose calculation has been used with the kernel. The kernel this study has employed is different in concept.

It is not possible to directly compare our study with the prior studies discussed in the Introduction in terms of accuracy and time of calculation, unless one uses the same condition of calculation such as radiation fields, phantom, the distance to EPID, methods of evaluation, and computing algorithms. The accuracy of our EPID model, however, can be clearly and independently shown by Figs. 5–7 which employed open fields and a flat phantom. The accuracy of the EPID model determines the accuracy of transit dosimetry and dose reconstruction.

#### IV. CONCLUSION

This study has developed a density-scaled layer model of EPID and applied it to transit dosimetry and dose reconstruction using our algorithm of dose reconstruction.<sup>18</sup> The model is based on layer description of actual components of EPID while using the densities of actual components within the XVMC code for fast calculations (less than 1 min for a beam). The use of layer modeling of EPID components produced discrepancies in penumbra dose calculations. This was reduced by a few percent by imposing a Gaussian kernel to measured EPID dose images. The developed model with the kernel was successfully utilized with full-scope Monte Carlo calculations for accurate and fast forward validation of radiation delivery in EPID and inverse dose reconstruction in a patient. The use of field-size independent, but phantom-thickness dependent calibration factors (image to dose) may be further optimized and simplified. The developed model with our algorithm of dose reconstruction<sup>18</sup> may find its use with the ongoing utilization of EPID and Monte Carlo methods for treatment planning.

#### ACKNOWLEDGMENTS

J. O. Kim expresses gratitude to Dr. Fippel for providing him with the XVMC code. We acknowledge the help of Dr. Jimm Grimm who designed the median filter used in this study and Dr. Byungyong Yi who provided the inhouse software for the 3D gamma analysis. The dose evaluation in this study was performed using MapCHECK (Sun Nuclear, Inc., Melbourne, FL). This study was in part supported by Varian Medical Systems, Inc. The method of dose reconstruction used in this study is US-patented.

- <sup>a)</sup> Author to whom correspondence should be addressed. Electronic mail: medicphys@hotmail.com; Telephone: 909 558 4904.
- <sup>1</sup> P. A. Jursinic and B. Nelms, "A 2-D diode array and analysis software for verification of intensity modulated radiation therapy delivery," *Med. Phys.* **30**, 870–879 (2003).
- <sup>2</sup> S. Amerio et al., "Dosimetric characterization of a large area pixel-segmented ionization chamber," *Med. Phys.* **31**, 414–420 (2004).
- <sup>3</sup> E. Spezi, A. L. Angelini, F. Romani, and A. Ferri, "Characterization of a 2D ion chamber array for the verification of radiotherapy treatments," *Phys. Med. Biol.* **50**, 3361–3373 (2005).
- <sup>4</sup> J. Kozelka, D. Savitskij, J. Robinson, B. Nelms, G. Zhang, and V. Feygelman, "Optimizing the accuracy of a helical diode array dosimeter: A comprehensive calibration methodology coupled with a novel virtual inclinometer," *Med. Phys.* **38**, 5021–5032 (2011).
- <sup>5</sup> J. V. Siebers, J. O. Kim, L. Ko, P. J. Keall, and R. Mohan, "Monte Carlo computation of dosimetric amorphous silicon electronic portal images," *Med. Phys.* **31**, 2135–2146 (2004).
- <sup>6</sup> E. Spezi and D. G. Lewis, "Full forward Monte Carlo calculation of portal dose from MLC collimated treatment beams," *Phys. Med. Biol.* **47**, 377–390 (2002).
- <sup>7</sup> T. R. McNutt, R. R. Mackie, P. Reckwerdt, N. Papanikolaou, and B. R. Paliwal, "Calculation of portal dose using the convolution/superposition method," *Med. Phys.* **23**, 527–535 (1996).
- <sup>8</sup> T. R. McNutt, R. R. Mackie, P. Reckwerdt, and B. R. Paliwal, "Modeling dose distributions from portal dose images using the convolution/superposition method," *Med. Phys.* **23**, 1381–1392 (1996).
- <sup>9</sup> C. V. Dahlgren, K. Eilertsen, T. D. Jorgensen, and A. Ahnesjo, "Portal dose image verification: the collapsed cone superposition method applied with different electronic portal imaging devices," *Phys. Med. Biol.* **51**, 335–349 (2006).
- <sup>10</sup> P. Reich, E. Bezak, M. Mohammadi, and L. Fog, "The prediction of transmitted dose distributions using a 3D treatment planning system Australas," *Phys. Eng. Sci. Med.* **29**, 18–29 (2006).
- <sup>11</sup> W. J. Van Elmpt, S. M. Nijsten, B. J. Mijnheer, and A. W. Minken, "Experimental verification of a portal dose prediction model," *Med. Phys.* **32**, 2805–2818 (2005).
- <sup>12</sup> W. Van Elmpt et al., "3D in vivo dosimetry using megavoltage cone-beam CT and EPID dosimetry," *Int. J. Radiat. Oncol., Biol., Phys.* **73**, 1580–1587 (2009).
- <sup>13</sup> K. L. Pasma, B. J. M. Heijmen, M. Kroonwijk, and A. G. Visser, "Portal dose image (PDI) prediction for dosimetric treatment verification in radiotherapy. I. An algorithm for open beams," *Med. Phys.* **25**, 830–840 (1998).
- <sup>14</sup> R. J. W. Louwe, E. M. F. Damen, M. van Herk, W. H. Minken, O. Torzsok, and B. J. Mijnheer, "Three-dimensional dose reconstruction of breast cancer treatment using portal imaging," *Med. Phys.* **30**, 2376–2389 (2003).
- <sup>15</sup> B. Warkentin, S. Steciw, S. Rathee, and B. G. Fallone, "Dosimetric IMRT verification with a flat-panel EPID," *Med. Phys.* **33**, 3143–3155 (2003).
- <sup>16</sup> S. M. Nijsten, A. W. Minken, P. Lambin, and I. A. Bruinvis, "Verification of treatment parameter transfer by means of electronic portal dosimetry," *Med. Phys.* **31**, 341–347 (2004).
- <sup>17</sup> M. Wendling, R. J. Louwe, L. N. McDermott, J. J. Sonke, M. van Herk, and B. J. Mijnheer, "Accurate two-dimensional IMRT verification using a back-projection EPID dosimetry method," *Med. Phys.* **33**, 259–273 (2006).
- <sup>18</sup> I. J. Yeo, J. W. Jung, M. Chew, J. O. Kim, B. Wang, S. DiBiase, Y. Zhu, and D. Lee, "Dose reconstruction for intensity-modulated radiation therapy using a non-iterative method and portal dose image," *Phys. Med. Biol.* **54**, 5223–5236 (2009).
- <sup>19</sup> M. Patridge, M. Ebert, and B.-M. Hesse, "IMRT verification by three-dimensional dose reconstruction from portal beam measurements," *Med. Phys.* **29**, 1847–1858 (2002).
- <sup>20</sup> B. M. C. McCurdy, K. Luchka, and S. Pistorius, "Dosimetric investigation and portal dose image prediction using an amorphous silicon electronic portal imaging device," *Med. Phys.* **28**, 911–924 (2001).
- <sup>21</sup> B. M. C. McCurdy and S. Pistorius, "A two-step algorithm for predicting portal dose images in arbitrary detectors," *Med. Phys.* **7**, 2109–2116 (2000).
- <sup>22</sup> E. J. Morton, W. Swindell, D. G. Lewis, and P. M. Evans, "A linear diode scintillation crystal-photodiode detector for megavoltage imaging," *Med. Phys.* **18**, 681–691 (1991).
- <sup>23</sup> V. N. Hansen, W. Swindell, and P. M. Evans, "Extraction of primary signal from EPIDs using only forward convolution," *Med. Phys.* **24**, 1477–1484 (1997).
- <sup>24</sup> L. Spies, M. Patridge, B. A. Groh, and T. Bortfeld, "An iterative algorithm for reconstructing incident beam distributions from transmission measurements using electronic portal imaging," *Phys. Med. Biol.* **46**, N203–N211 (2001).
- <sup>25</sup> W. Van Elmpt, S. Nijsten, and R. Schiffeleers, "A Monte Carlo based three-dimensional dose reconstruction method derived from portal dose images," *Med. Phys.* **33**, 2426–2434 (2006).
- <sup>26</sup> S. Steciw, B. Warkentin, S. Rathee, and B. G. Fallone, "Three-dimensional IMRT verification with a flat-panel EPID," *Med. Phys.* **32**, 600–612 (2005).
- <sup>27</sup> G. Jarry and F. Verhaegen, "Patient-specific dosimetry of conventional and intensity modulated radiation therapy using a novel full Monte Carlo phase space reconstruction method from electronic portal images," *Phys. Med. Biol.* **52**, 2277–2299 (2007).
- <sup>28</sup> M. Fippel, "Fast Monte Carlo dose calculation for photon beams based on the VMC electron algorithm," *Med. Phys.* **26**, 1466–1475 (1999).
- <sup>29</sup> L. Ko, J. O. Kim, and J. Siebers, "Investigation of the optimal backscatter for an aSi electronic portal imaging device," *Phys. Med. Biol.* **49**, 1723–1738 (2004).
- <sup>30</sup> D. A. Low, W. B. Harms, S. Mutic, and J. A. Purdy, "A technique for the quantitative evaluation of dose distributions," *Med. Phys.* **25**, 656–661 (1998).